

3D Ice Shape Description Method Based on BLSOM Neural Network

ZHU Bailiu¹, ZUO Chenglin^{2*}

1. AVIC General Huanan Aircraft Industry Co., Ltd., Zhuhai 519040, P. R. China;

2. Key Laboratory of Icing and Anti/De-icing, China Aerodynamics Research and Development Center, Mianyang 621000, P. R. China

(Received 11 July 2023; revised 15 March 2024; accepted 15 June 2024)

Abstract: When checking the ice shape calculation software, its accuracy is judged based on the proximity between the calculated ice shape and the typical test ice shape. Therefore, determining the typical test ice shape becomes the key task of the icing wind tunnel tests. In the icing wind tunnel test of the tail wing model of a large amphibious aircraft, in order to obtain accurate typical test ice shape, the Romer Absolute Scanner is used to obtain the 3D point cloud data of the ice shape on the tail wing model. Then, the batch-learning self-organizing map (BLSOM) neural network is used to obtain the 2D average ice shape along the model direction based on the 3D point cloud data of the ice shape, while its tolerance band is calculated using the probabilistic statistical method. The results show that the combination of 2D average ice shape and its tolerance band can represent the 3D characteristics of the test ice shape effectively, which can be used as the typical test ice shape for comparative analysis with the calculated ice shape.

Key words: icing wind tunnel test; ice shape; batch-learning self-organizing map; neural network; 3D point cloud

CLC number: V211.79

Document code: A

Article ID: 1005-1120(2024)S-0070-11

0 Introduction

In order to check the ice shape calculation software, it is necessary to compare and analyze the calculated ice shape with the typical test ice shape to judge its accuracy. When determining the typical test ice shape, there are two problems: One is how to identify the typical characteristics of the test ice shape, and the other is how to accurately and comprehensively describe and record the 3D test ice shape data. To solve these two problems, many efforts have been made.

Ref.[1] defined the ice shape parameters and pointed out that the angle of the upper ice angle was directly related to the maximum lift, drag and pitching moment. Working Group 12A believed that the higher the projection height of the upper ice angle in the lift direction, the more critical the ice shape^[2].

The geometric parameters of the ice shape are

directly related to the aerodynamic effect of the ice shape on the aircraft. The method of recording the 2D ice shape in the icing wind tunnel test is usually to draw the ice shape section on the card-board with a pencil^[3]. Moreover, for the icing wind tunnel test of 2D models, even if the quality of the icing wind tunnel fully meets the requirements of the industry standard^[4], the spatial heterogeneity and temporal instability of the flow field, cloud field and temperature field can also lead to significant changes in the ice shape along the model direction. However, it will lose the 3D details of the ice shape. The mold and casting method method can completely reproduce the 3D details of the ice shape^[5], but it also has many disadvantages, such as too much processing time^[3], difficult to scale and digitize^[6].

In 2012, NASA's Ice Research Department proposed a research plan to develop and verify the technology of using commercial laser scanners to re-

*Corresponding author, E-mail address: zhubl003@avic.com.

How to cite this article: ZHU Bailiu, ZUO Chenglin. 3D ice shape description method based on BLSOM neural network[J]. Transactions of Nanjing University of Aeronautics and Astronautics, 2024, 41(S): 70-80.

<http://dx.doi.org/10.16356/j.1005-1120.2024.S.009>

cord full 3D ice shape. The plan is divided into two stages. The first stage is to select laser scanners and post-processing software, and the second stage is to verify the selected hardware and software through a series of tests. At present, the first phase has been completed. The selected scanner is the Romer Absolute Scanner, and the selected data processing software is Geomagic^[3].

In order to verify the effectiveness of the laser scanning/rapid prototyping technology, Ref.[6] completed the icing test in the NASA IRT icing wind tunnel, and successively used the laser scanning/rapid prototyping technology and the mold and casting method to produce the artificial 3D ice shape, and determined the consistency of the two sets of ice shape geometry through comparison. Ref.[7] compared the difference between the two sets of ice shapes through the force-measuring test with ice shape in the dry air wind tunnel. The results showed that the accuracy of the laser scanning/rapid prototyping technology can meet the usage requirements. Refs.[8-9] used pressure-sensitive paint to compare the pressure distribution on the surface of the model with two sets of ice shapes installed respectively in the dry air wind tunnel. The results showed that the consistency of the pressure distribution induced by the two sets of ice shapes was quite good.

The laser scanning/rapid prototyping technology can record full 3D ice shape, and has more advantages than the traditional mold and casting method in terms of convenience and accuracy. However, since the comparison between the calculated ice shape and the test ice shape is usually carried out on a 2D profile, the laser scanning/rapid prototyping technology cannot be directly used to determine the typical test ice shape.

If the 2D ice shape is cut directly from the 3D ice shape by the Romer Absolute Scanner, it will be the same as the aforementioned method of manually drawing ice shape section. The self-organizing map (SOM) neural network technology can be used to cluster 3D data of the ice shape on the 2D plane, so that a small number of 2D data can be used to repre-

sent the overall trend of 3D ones. Therefore, the 2D average ice shape along the development direction of 3D ice shape can be obtained, while its tolerance band can also be calculated by using the probabilistic statistical analysis method. The combination of average ice shape and its tolerance band can reflect all information of 3D ice shape, and thus can be used as a new description method of 3D ice shape.

Refs.[10-13] used SOM neural network to describe the ice shape or its roughness. Besides, researchers also used SOM neural network technology to study point cloud data reconstruction^[14], customer management^[15], information retrieval^[16], data mining^[17-19] and other issues.

In this study, the icing wind tunnel tests of a large amphibious aircraft were carried out at the 3 m×2 m icing wind tunnel of China Aerodynamic Research and Development Center (CARD C). During the tests, the Romer Absolute Scanner was used to measure the test ice shape, and the 3D point cloud data of the ice shape was obtained. Furthermore, the batch-learning self-organizing map (BLSOM) neural network method was used to process the 3D point cloud data into a 2D average ice shape along the model spanning direction, while its tolerance band was obtained by using the probabilistic statistical method. The results show that the combination of 2D average ice shape and its tolerance band can effectively represent the 3D characteristics of the test ice shape, which can be used as the typical test ice shape for comparative analysis with the calculated ice shape.

1 BLSOM

SOM neural network is an important class of unsupervised learning methods, which can be used for clustering, high-dimensional visualization, data compression, feature extraction and other purposes. It integrates a large number of signal processing mechanisms of the human neurons, and has unique structural characteristics. The standard SOM^[20-22] was proposed by Teuvo Kohonen in 1981, so it is also called Kohonen Network.

Based on the standard SOM, Abe and Kanaya

et al. developed the BLSOM neural network^[22-24], which is mainly used for gene classification currently^[23-25]. In this method, the initial value of the neural network array is determined by the principal component analysis (PCA)^[24]. Compared with SOM which randomly determines the initial value of the neural network array, the mapping results of BLSOM do not depend on the order of input data in the learning process. Besides, BLSOM can also realize the parallel processing of large-scale data in the learning process.

There are three key points to note when using BLSOM to describe 3D ice shapes. Firstly, the experimental model should be an equal-straight segment model, which means that the geometric shape of the model is formed by directly stretching a 2D airfoil along the normal direction. In theory, this model should produce exactly the same ice shape across all sections. But in fact, due to various factors, the ice shapes of each cross section along the spanwise direction usually have significant differences. Secondly, the topological structure of BLSOM can be either 1D linear array or 2D planar array. However, when applying it to describe the 3D ice shape, the topological structure of one-dimensional linear array is more appropriate. Thirdly, it is necessary to determine the number of neurons based on the actual ice shape. If the number of neurons is too small, it is not possible to fully capture the ice shape characteristics. If the number of neurons is too large, it will lead to a disordered average ice shape.

The detailed steps for using BLSOM to process the 3D point cloud data of the ice shape are as follows:

(1) Project the 3D point cloud data of the ice shape onto the 2D plane along the spanwise direction to obtain the input dataset X .

(2) Select 1D linear array as the topological structure of BLSOM. The number of neurons is set to M , while the learning times is set to 1 000.

(3) Determine the initial weight vector of neurons using PCA, as shown in Fig.1.

$$\mathbf{b}^i = \mathbf{X}_{av} + 5 \times \sigma_1 \times T_1 \times \frac{i - M/2}{M} \quad (1)$$

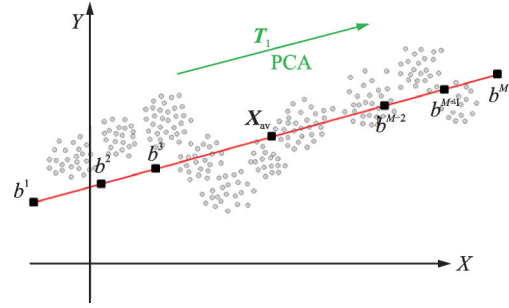


Fig.1 Initial value of neural network array determined by PCA

where \mathbf{b}^i is the weight vector of the i th neuron and \mathbf{X}_{av} the average vector of the dataset X ; σ_1 and T_1 are the standard deviation and feature vectors of the first principal component determined by PCA.

(4) Assign the data in dataset X to adjacent neurons to form M clusters, and update the neuron weight vector as

$$\mathbf{b}_{new}^i = \mathbf{b}^i + \alpha(r) \times (\mathbf{X}_{av}^i - \mathbf{b}^i) \quad (2)$$

where \mathbf{X}_{av}^i represents the position average vector of all data allocated by the i th neuron and $\alpha(r)$ the r th learning efficiency, which is determined as

$$\alpha(r) = \max\{0.01, 0.06 \times (1 - r/1000)\} \quad (3)$$

(5) After learning with 1 000 times, the final weight vectors of M neurons are obtained, and each neuron is located in the center of its cluster.

Compared with SOM, BLSOM has two obvious advantages. First, since the initial value of neurons is calculated by PCA, neurons can always maintain their own topological structure during the learning process (Fig.2). Second, the original dataset X participates in the calculation in a holistic manner, the learning process of neurons can achieve large-scale parallel computing, greatly improving computational efficiency.

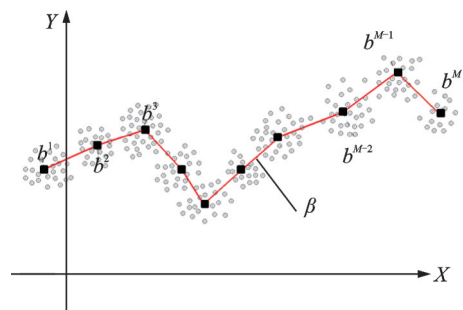


Fig.2 Manifold determined by BLSOM

As shown in Fig.2, a manifold β is formed by connecting neurons using linear segments according to their own topological structure. In the processing of the 3D point cloud data of the ice shape, manifold β is referred to the 2D average ice shape along the spanwise direction of the model from its 3D ice shape.

2 Tolerance Band Calculation for Average Ice Shape

In Fig.2, BLSOM is used to cluster the point cloud data to form a series of clusters, each of which is represented by a winning neuron located in the center. Therefore, the standard deviation of the data in the cluster relative to the winning neuron represents its dispersion, which can be used to represent the uncertainty of the winning neuron.

Fig.3 shows the winning neuron b^n and its two adjacent neurons b^{n-1} and b^{n+1} on manifold β . In this paper, it is assumed that manifold β is the first order manifold in the 2D space, characterized by the fact that the local slope of manifold β at neuron b^n is equal to the slope of a straight line determined by the two closest neurons b^{n-1} and b^{n+1} . Assume that all deviations of the point cloud data from manifold β are perpendicular to manifold β , which means that the deviation between arbitrary point cloud data and manifold β is equal to the projection height in the normal direction of its winning neuron b^n .

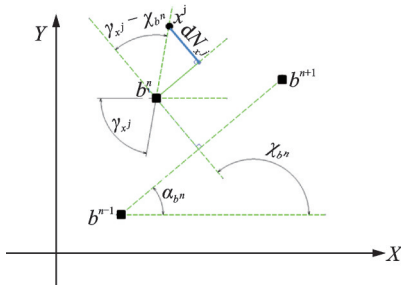


Fig.3 Projection of point cloud data

In Fig.3, α_{b^n} represents the angle between vector $b^{n-1}b^{n+1}$ and the X-axis, which is the tangential angle of manifold β at neuron b^n . As shown in Fig.4, when the vector $b^{n-1}b^{n+1}$ is located in the first and fourth quadrants of the XY coordinate

plane, $\alpha_{b^n} \in (-\pi/2, \pi/2)$, α_{b^n} can be directly obtained from the inverse tangent function. When the vector $b^{n-1}b^{n+1}$ is located in the second and third quadrants of the XY coordinate plane, $\alpha_{b^n} \in (\pi/2, 3\pi/2)$, it is necessary to add π to the arc-tangent function value to obtain the correct α_{b^n} . Therefore, the complete expression for α_{b^n} is shown as

$$\alpha_{b^n} = \begin{cases} \arctan\left(\frac{y_{b^{n+1}} - y_{b^{n-1}}}{x_{b^{n+1}} - x_{b^{n-1}}}\right) & x_{b^{n+1}} > x_{b^{n-1}} \\ \arctan\left(\frac{y_{b^{n+1}} - y_{b^{n-1}}}{x_{b^{n+1}} - x_{b^{n-1}}}\right) + \pi & x_{b^{n+1}} < x_{b^{n-1}} \\ -\frac{\pi}{2} & x_{b^{n+1}} = x_{b^{n-1}}, y_{b^{n+1}} < y_{b^{n-1}} \\ \frac{\pi}{2} & x_{b^{n+1}} = x_{b^{n-1}}, y_{b^{n+1}} \geq y_{b^{n-1}} \end{cases} \quad (4)$$

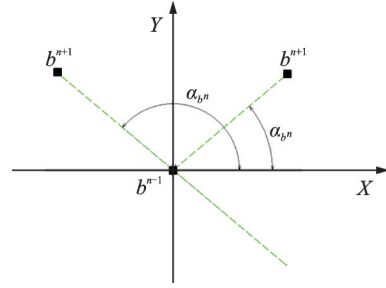


Fig.4 Definition of α_{b^n} angle

As can be seen from Fig.3, the normal angle χ_{b^n} of manifold β at neuron b^n can be described as $\chi_{b^n} = \alpha_{b^n} + \pi/2$. For the point x^j , its direction angle γ_{x^j} relative to the neuron b^n can be calculated as

$$\gamma_{x^j} = \begin{cases} \arctan\left(\frac{y_{x^j} - y_{b^n}}{x_{x^j} - x_{b^n}}\right) & x_{x^j} > x_{b^n} \\ \arctan\left(\frac{y_{x^j} - y_{b^n}}{x_{x^j} - x_{b^n}}\right) + \pi & x_{x^j} < x_{b^n} \\ -\frac{\pi}{2} & x_{x^j} = x_{b^n}, y_{x^j} < y_{b^n} \\ \frac{\pi}{2} & x_{x^j} = x_{b^n}, y_{x^j} \geq y_{b^n} \end{cases} \quad (5)$$

Therefore, the normal projection height dN_{x^j} of the point x^j relative to the manifold β at the neuron b^n is calculated as

$$dN_{x^j} = h \cdot \cos(\gamma_{x^j} - \chi_{b^n}) \quad (6)$$

where $h = \left[(x_{x^j} - x_{b^n})^2 + (y_{x^j} - y_{b^n})^2 \right]^{1/2}$ is the linear distance between the point x^j and the neuron b^n .

The normal projection height of all points in the clusters relative to the manifold β can be used to calculate the uncertainty of the corresponding winning neuron. In this study, it is assumed that the position deviation of the points in the cluster relative to the winning neuron obeys the normal distribution. Fig.5 shows the average ice shape with its tolerance band. The average ice shape is obtained by connecting all neurons, and the tolerance band is obtained by connecting the inner and outer boundaries of the 95% confidence interval of all neurons. In the comparison of the calculated ice shape and the test ice shape, if the upper and lower corners of the calculated ice shape locate in the tolerance band, it can be argued that the calculated ice shape and the test ice shape have similar aerodynamic effects on the aircraft.

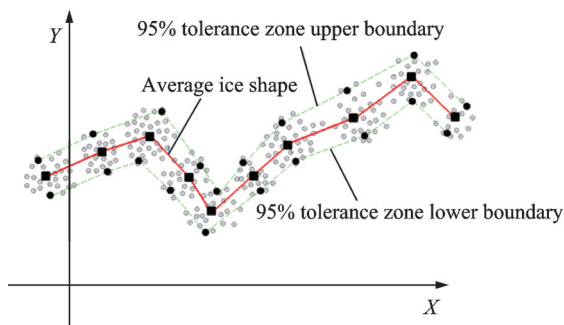


Fig.5 Average ice shape and its tolerance band

3 Experimental Results and Discussion

The icing tests were performed in the $3\text{ m} \times 2\text{ m}$ icing wind tunnel at CARDC. The test model HS2 was the flat tail airfoil of a large amphibious aircraft, which was formed by stretching the 2D airfoil for 2 m in the vertical direction. The model was vertically installed in the middle of the wind tunnel test section.

The test condition numbered HS2-02 is as follows: The simulated altitude is 4 500 m, the air velocity is 105.56 m/s, the model's angle of attack is 2.15° , the static air temperature is -1.25°C , the total air temperature is -6.8°C , the median volumetric diameter is $20\ \mu\text{m}$, the liquid water content is $0.49\ \text{g}/\text{m}^3$, and the icing spray time is 22.5 min. In order to investigate the repeatability of the icing test, another icing test numbered HS2-09 was conducted,

which had the same test condition with HS2-02.

Fig.6 shows the comparison of the ice shape in the test HS2-02 and HS2-09. Generally, the ice shape of the two tests agreed with each other well. For the areas near the wind tunnel wall at the top and bottom of the model, due to the mutual interference between the wall and the model, the distributions of the flow field and cloud field in these areas were uneven, thereby resulting in quite different ice shapes. Therefore, ice shape recording should avoid these areas. In the tests, the quality of the flow field, the temperature field, and the cloud field at the height range of 500 mm to 1 500 mm meets the relevant requirements of SAE APR 5905, and the ice shape in this area was effective. Therefore, four 2D ice profiles were obtained at the height of 500, 1 000, 1 100, and 1 500 mm by using hand tracing.

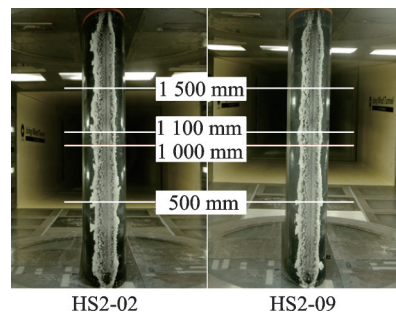


Fig.6 Comparison of ice shape in the tests

3.1 2D ice shape

Fig.7 shows the comparison of the 2D ice profiles at four different locations in the HS2-02 test. Since the test model was made of a single airfoil directly stretched in the vertical direction, the four ice profiles should be identical in theory. However, in practice, since the flow field, the temperature field and the cloud field could not be at absolutely uniform distribution, the ice shape at different locations would have differences, which means that the test ice shape has significant 3D characteristics. As can be seen in Fig.7, the four ice profiles have obvious differences, especially for the two ice profiles at the heights of 1 500 mm and 1 100 mm.

Fig.8 shows the comparison of the 2D ice profiles at four different locations in the test HS2-09. Similarly, the four ice profiles were different obviously.

Therefore, how to select the accurate and appropriate 2D test ice shape becomes a difficult problem when comparing it with the results calculated by the ice shape calculation software. Since the ice profiles obtained by hand tracing cannot reflect the full 3D characteristics of the ice shape, it cannot be used to determine the typical ice shape effectively.

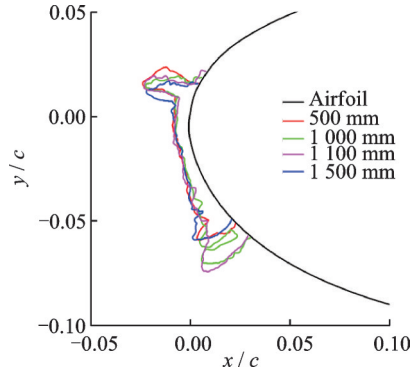


Fig.7 Comparison of ice profile in the test HS2-02

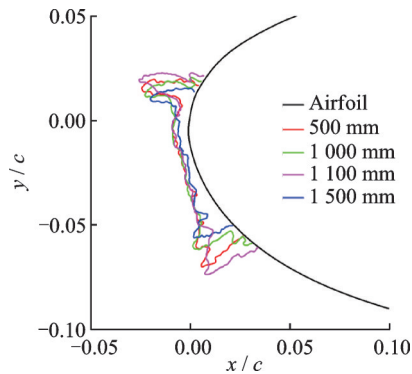
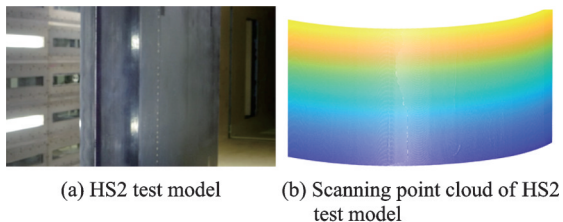


Fig.8 Comparison of ice profile in the test HS2-09

3.2 3D ice shape

The Romer Absolute Scanner was used to obtain the 3D ice shape with the height range of 121 mm. Fig.9 shows the test model and its 3D

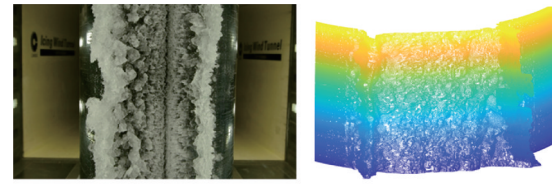


(c) 3D point cloud projected to XY plane of HS2 model

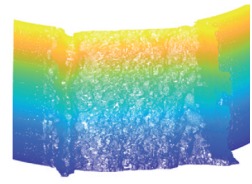
Fig.9 Test model and its 3D shape

shape. The amount of the 3D points of the model shape was 601 619, and their average distance was 0.252 2 mm.

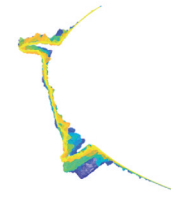
Fig.10 and Fig.11 show the actual test ice and its corresponding 3D ice shape measured by the Romer Absolute Scanner in the test HS2-02 and HS2-09. The amount of the 3D ice shape points were 847 329 and 988 733, while their average distance were 0.267 5 mm and 0.268 3 mm.



(a) HS2-02 test ice shape



(b) HS2-02 3D ice-shaped scanning point cloud

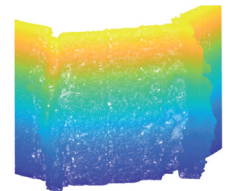


(c) HS2-02 3D point cloud projected to XY plane

Fig.10 Actual ice and its 3D shape in the test HS2-02



(a) HS2-09 test ice shape



(b) HS2-09 3D ice-shaped scanning point cloud



(c) HS2-09 3D point cloud projected to XY plane

Fig.11 Actual ice and its 3D shape in the test HS2-09

3.3 Average ice shape and tolerance band

Fig.12 shows the 2D average shape and its tolerance band calculated by using BLSOM based on the 3D model shape points. Since the surface of the test model is not covered with any shape, the calculated 2D average shape actually describes the shape characteristics of the test model.

Overall, the average shape and its tolerance

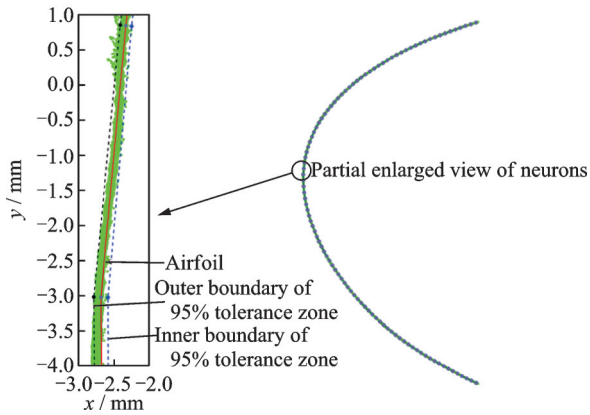


Fig.12 Average shape and the tolerance band of the test model

band are smooth and slender, which accurately describe the shape of the test model. It can be seen from the enlarged image that, the average shape is located in the middle of the points, and a 95% probability tolerance band is located on both sides of the average shape, covering most of the point cloud area. The average shape has the arc length of about 356.42 mm, and the average width of the tolerance band is about 0.15 mm, which is determined by the manufacturing error of the model and the measurement error of the scanner.

When using the BLSOM to describe the 3D test ice shape, the number of neurons should be determined according to the actual ice shape. As shown in Fig.13, three average ice shapes are obtained by using BLSOM with 15, 30 and 50 neurons respectively in the test HS2-02. In Fig.13(a), the average ice shape is clear but does not capture the upper and lower ice corners well. In Fig.13(b), not only the average ice shape is clear, but also the upper and lower ice corners are captured well. In Fig.13(c), the average ice shape obtains the best upper and the lower ice corners, but its structure is relatively messy. Therefore, by comparison, the neural network with 30 neurons could describe the ice shape best.

Fig.14 shows the average ice shape and its 95% probability tolerance band in the test HS2-02. It can be seen that each neuron is located at the center of its point cluster, and the average ice shape represents the trend of 2D point cloud data. At the upper and lower ice corners, which have the great-

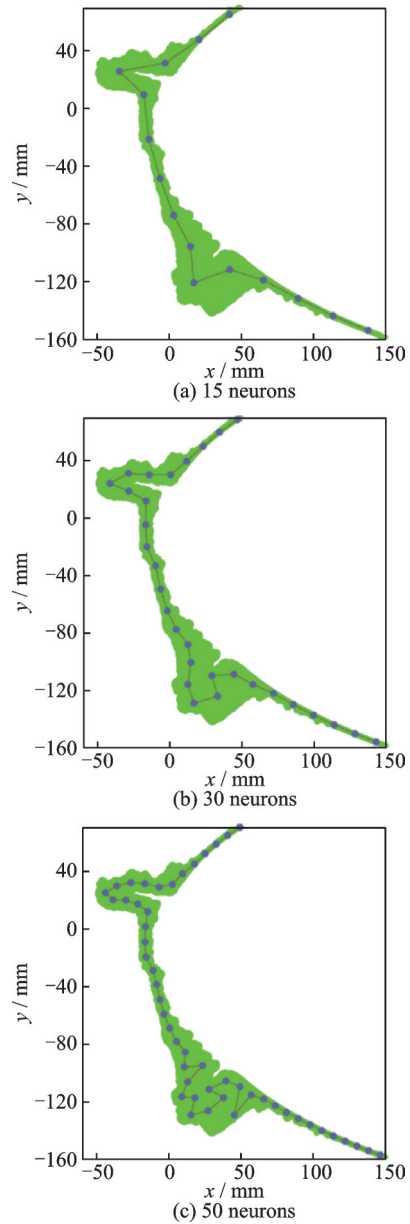


Fig.13 Average ice shapes by using BLSOM with different number of neurons

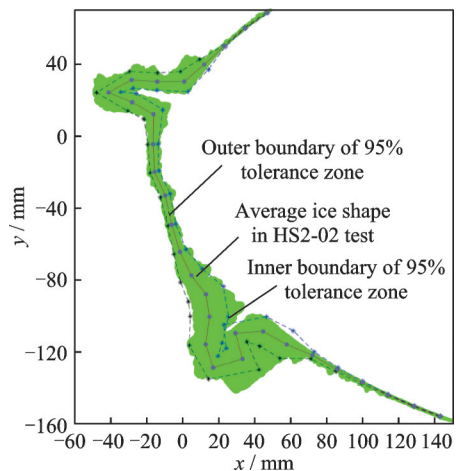


Fig.14 Average ice shape and its tolerance band in the test HS2-02

est impact on aerodynamic forces, the distribution of point cloud data is relatively scattered, and the 95% probability tolerance band can cover most of the point cloud area. In the lower regions with low ice content, the tolerance band range is sharply narrowed, and the average ice shape and its tolerance band outline the model shape.

Fig.15 shows the comparison of the average ice shape and the 2D ice profiles at four locations in the test HS2-02. It can be seen that the trend of the average ice shape and the 2D ice profiles at four locations are roughly the same, and the 95% probability tolerance band basically encloses the 2D ice profiles at four locations. Generally, the average ice shape calculated by BLSOM and its 95% probability tolerance band can represent all information contained in the 3D ice shape of the test HS2-02.

Fig.16 shows the average ice shape and its

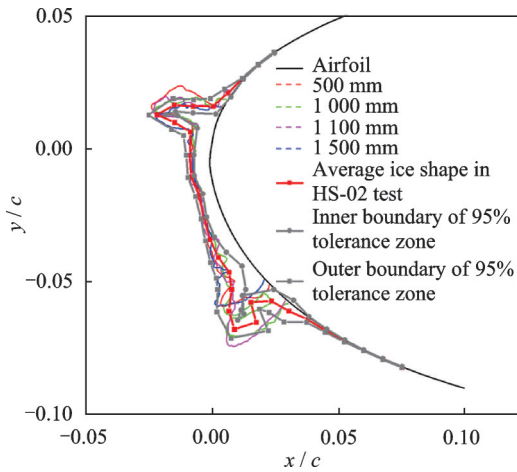


Fig.15 Comparison of ice profile in the test HS2-02

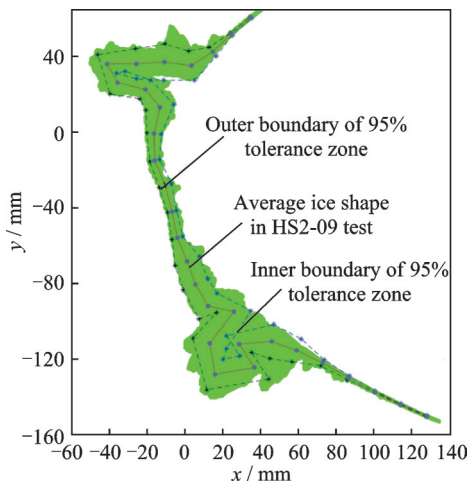


Fig.16 Average ice shape and its tolerance band in the test HS2-09

95% probability tolerance band in the test HS2-09, while Fig.17 shows the comparison between the average ice shape and the 2D ice profiles at four locations. Similarly, the average ice shape calculated by BLSOM and its 95% probability tolerance band can effectively represent all information contained in the 3D ice shape of the test HS2-09.

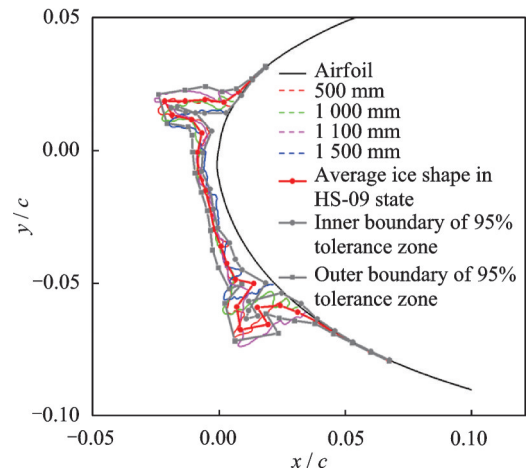


Fig.17 Comparison of ice profile in the test HS2-09

3.4 Overlap of average ice shapes

In statistics, multiple measurements and their arithmetic mean can eliminate the randomness error of measuring. Therefore, in this study, the measured 3D ice shape points in the test HS2-02 and HS2-09 are overlapped together, base on which the average ice shape and its tolerance band are calculated by using BLSOM.

Fig.18 shows the comparison of the calculated

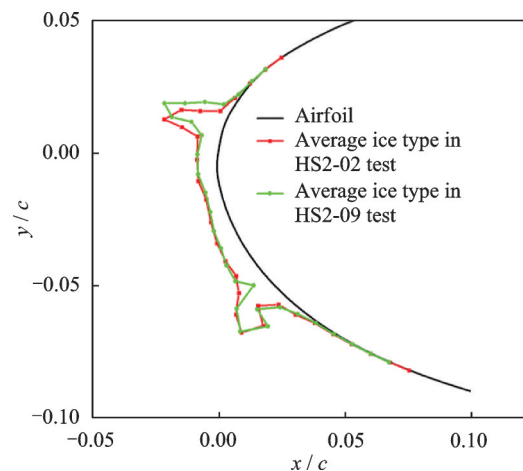


Fig.18 Comparison of average ice shapes in the tests HS2-02 and HS2-09

average ice shapes in the tests HS2-02 and HS2-09. Fig.19 shows the overlapped 3D ice shape points. Fig.20 shows the average ice shape and its tolerance band calculated based on the overlapped 3D points. Consistent with previous analysis, the average ice shape and its tolerance band can also represent all information contained in the 3D ice shape.

Fig.21 shows the comparison of the average ice shapes. It can be seen that the height of the upper

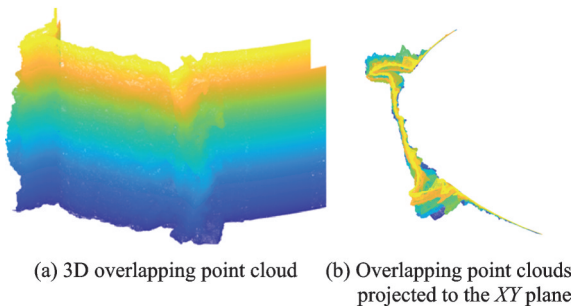


Fig.19 Overlapped 3D ice shape points

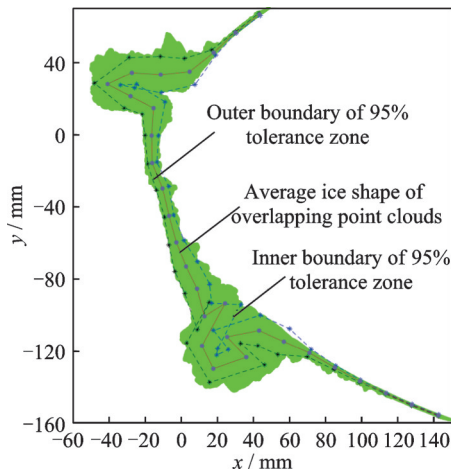


Fig.20 Average ice shape and its tolerance band in overlapping state

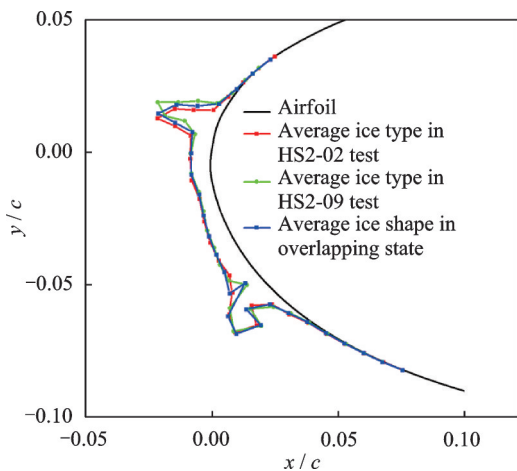


Fig.21 Comparison of average ice shapes in different states

ice horn in the overlapping state is between the height of the upper ice horn in the tests HS2-02 and HS2-09. In the upper region of the lower ice horn, the average ice shape in the overlapping state is more similar to that in HS2-09. In most of the remaining areas, the average ice shape of the three states almost coincide with each other.

Obviously, increasing the number of ice tests with the same condition can obtain more ice shape data. Therefore, the average ice shape and its tolerance band calculated after overlapping the ice shapes can more accurately describe the characteristics of the 3D ice shape in the test, which can be used as the typical test ice shape for comparative analysis with the calculated ice shape.

4 Conclusions

Compared with other ice shape description methods, the main advantages of our proposed BLSOM based 3D ice shape description method include:

(1) Compared with hand tracing method, our proposed method can record the changes in ice shape along the spanwise direction, which can reflect all information about the 3D ice shape. Therefore, the combination of the 2D average ice shape and its tolerance band can be used as the typical test ice shape better.

(2) Compared with the mold and casting method, our proposed method can record the 3D ice shape in a numerical manner, and convert it into 2D ice shape data for subsequent usage. In addition, by overlapping the 3D ice shapes, the randomness error of measuring can be eliminated.

In the future work, the BLSOM based 3D ice shape description method can be improved in the following aspects:

(1) To develop an accurate point cloud data alignment method to reduce the deviation of their overlapping.

(2) To enable the number of neurons to automatically adjust with the curvature change of the ice shape.

References

- [1] WRIGHT W B, CHUNG J. Correlation between geometric similarity of ice shapes and the resulting aerodynamic performance degradation—A preliminary investigation using WIND: AIAA-2000-0097[R]. [S.l.]: AIAA, 2000.
- [2] U S Department of Transportation. Report of the 12A Working Group on determination of critical ice shapes for the certification of aircraft: DOT/FAA/AR-00/37 [R]. Washington DC, USA: Federal Aviation Administration, 2000.
- [3] LEE S, BROEREN A P, ADDY H E, et al. Development of 3D ice accretion measurement method: AIAA 2012-2938[R]. [S.l.]: AIAA, 2012.
- [4] AC-9C Aircraft Icing Technology Committee. Calibration and acceptance of icing wind tunnels: SAE APR 5905[R]. [S.l.]: SAE, 2009.
- [5] REEHOEST A L, RICHTER G P. New methods and materials for molding and casting ice formations: NASA-TM-100126[R]. [S.l.]: NASA, 1987.
- [6] LEE S, BROEREN A P, KREEGER R E, et al. Implementation and validation of 3-D ice accretion measurement methodology: AIAA 2014-2613[R]. [S.l.]: AIAA, 2014.
- [7] BROEREN A P, ADDY H E J, LEE S, et al. Validation of 3-D ice accretion measurement methodology for experimental aerodynamic simulation: AIAA 2014-2614[R]. [S.l.]: AIAA, 2014.
- [8] MONASTERO M C, BRAGG M. Validation of 3-D ice accretion measurement methodology using pressure-sensitive paint: AIAA 2014-2615[R]. [S.l.]: AIAA, 2014.
- [9] MONASTERO M C. Validation of 3-D ice accretion documentation and replication method including pressure-sensitive paint[D]. Urbana: University of Illinois at Urbana-Champaign, 2013.
- [10] MCCLAIN S T, TINO P, KREEGER R E. Ice shape characterization using self-organizing maps: AIAA 2009-3865[R]. [S.l.]: AIAA, 2009.
- [11] MCCLAIN S T, KREEGER R E. Assessment of ice shape roughness using a self-organizing map approach: AIAA 2013-2546[R]. [S.l.]: AIAA, 2013.
- [12] MCCLAIN S T. Manual point cloud registration for combined ice roughness and ice thickness measurements: AIAA 2016-3590[R]. [S.l.]: AIAA, 2016.
- [13] NEUBAUER T, HASSLER W, PUFFING R. Ice shape roughness assessment based on a 3-D self-organizing map approach: AIAA 2020-2805[R]. [S.l.]: AIAA, 2013.
- [14] YANG W J. Logs of 3D image reconstruction based on 3D laser scanning technology[D]. Harbin: Northeast Forestry University, 2018. (in Chinese)
- [15] GUO Chonghui, ZHAO Zuwei. Customer segmentation and change mining based on customer behavior for 4S shop[C]//Proceedings of IEEE International Conference on Industrial Engineering and Engineering Management. [S.l.]: IEEE, 2015.
- [16] CHEN Guoyu. Research on Tianya BBS posts interfered with “Water Army” based on SOM—K-means clustering[D]. Wuhan: Huazhong University of Science and Technology, 2013. (in Chinese)
- [17] WANG Minglu. Clustering of generally distributed interval symbolic data using self-organizing map (SOM) algorithm[D]. Tianjin: Tianjin University, 2014. (in Chinese)
- [18] CAI Lihong. Improvement of SOM clustering algorithm and its application in text mining[D]. Nanjing: Nanjing University of Aeronautics and Astronautics, 2011. (in Chinese)
- [19] YUE Suqing. Research on SOM neural network and its application in hydrological zoning[D]. Nanjing: Hohai University, 2006. (in Chinese)
- [20] KOHONEN T. Self-organized formation of topologically correct feature maps[M]. Cambridge, Massachusetts, USA: MIT Press, 1988.
- [21] KOHONEN T. The self-organizing map[J]. Proceedings of the IEEE, 1990, 78(9): 1464-1480.
- [22] KOHONEN T, OJA E, SIMULA O, et al. Engineering applications of the self-organizing map[J]. Proceedings of the IEEE, 1996, 84(10): 1358-1384.
- [23] KANAYA S, KUDO Y, ABE T, et al. Gene classification by self-organization mapping of codon usage in bacteria with completely sequenced genome[J]. Genome Informatics, 1998(9): 369-371.
- [24] ABE T, KANAYA S, KINOCHI M, et al. Gene classification method based on batch-learning SOM[J]. Genome Informatics, 1999(10): 314-317.
- [25] KANAYA S, KINOCHI M, ABE T, et al. Analysis of codon usage diversity of bacterial genes with a self-organizing map (SOM): Characterization of horizontally transferred genes with emphasis on the E.coli O157 genome[J]. Gene, 2001, 276(1/2): 89-99.

Acknowledgement This work was supported by the AG600 project of AVIC General Huanan Aircraft Industry Co., Ltd.

Authors Mr. ZHU Bailiu obtained his master's degree from Beihang University in April 2007. In August 2010, he joined the General Department of Aviation Industry Tongfei South China Aircraft Industry Co., Ltd. as an engineer. His main research areas include aircraft aerodynamic testing, icing wind tunnel testing, and CFD.

Dr. ZUO Chenglin received his Ph.D. degree from National University of Defense Technology, China. He is now an

associate researcher at Key Laboratory of Icing and Anti/De-icing of CARDC. His research interests include computer vision, flow visualization and non-contact measurement.

Author contributions Mr. ZHU Bailiu designed this study, completed all the icing tests, compiled a complete calculation program, and compiled the original manuscript of the article. Dr. ZUO Chenglin proposed important revisions to the article and polished the English version of the article. The authors commented on the manuscript draft and approved the submission.

Competing interests The authors declare no competing interests.

(Production Editor: SUN Jing)

基于BLSOM神经网络的三维冰形描述方法

朱百六¹, 左成林²

(1. 中航通飞华南飞机工业有限公司, 珠海 519040, 中国;

2. 中国空气动力研究与发展中心结冰与防除冰重点实验室, 绵阳 621000, 中国)

摘要:在校核冰形计算软件时,根据计算冰形与典型试验冰形的接近程度来判断冰形计算软件是否准确,因此确定典型试验冰形就成为冰风洞试验的关键任务。在某大型水陆两栖飞机尾翼冰风洞试验中,为获得精确的典型试验冰形,使用Romer Absolute扫描仪获得了尾翼模型结冰冰形的三维点云数据,然后使用批学习自组织映射(Batch-learning self-organizing map, BLSOM)神经网络获得了冰形的三维点云数据沿模型展向的二维平均冰形,并使用概率统计方法获得了二维平均冰形的公差带。结果表明,二维平均冰形与其公差带相结合可准确代表试验冰形的三维特征信息,因此可作为一种典型试验冰形与计算冰形进行对比分析。

关键词:结冰风洞试验;冰形;批学习自组织映射;神经网络;三维点云